Journal of Electron Spectroscopy and Related Phenomena 185 (2012) 406–416

Contents lists available at SciVerse ScienceDirect

Journal of Electron Spectroscopy and Related Phenomena

journal homepage: www.elsevier.com/locate/elspec

Using X-PEEM to study biomaterials: Protein and peptide adsorption to a polystyrene–poly(methyl methacrylate)-b-polyacrylic acid blend

Bonnie O. Leung[a,1], Adam P. Hitchcock[a,*], Rena M. Cornelius[b], John L. Brash[b], Andreas Scholl[c], Andrew Doran[c]

[a] Chemistry and Chemical Biology, BIMR, McMaster University, Hamilton, ON, Canada L8S 4M1
[b] School of Biomedical Engineering, McMaster University, Hamilton, ON, Canada L8S 4M1
[c] Advanced Light Source, Berkeley Lab, Berkeley, CA 94720, USA

ARTICLE INFO

Article history:
Available online 18 June 2012

Keywords:
Photoemission electron microscopy
X-PEEM
NEXAFS
AFM
Mapping
Protein adsorption
HSA
Polystyrene
Poly(methyl methacrylate)-b-polyacrylic acid
Blend

ABSTRACT

Recent synchrotron-based soft X-ray photoemission electron microscopy (X-PEEM) studies of protein and peptide interaction with phase segregated and patterned polymer surfaces in the context of optimization of candidate biomaterials are reviewed and a study of a new system is reported. X-PEEM and atomic force microscopy (AFM) were used to investigate the morphology of a phase-segregated thin film of a polystyrene/poly(methyl methacrylate)-b-polyacrylic acid (PS/PMMA-PAA) blend, and its interactions with negatively charged human serum albumin (HSA) and positively charged SUB-6 (a cationic antimicrobial peptide, RWWKIWVIRWWR-NH_2) at several pHs. At neutral pH, where the polymer surface is partially negatively charged, HSA and SUB-6 peptide showed contrasting adsorption behavior which is interpreted in terms of differences in their electrostatic interactions with the polymer surface.
© 2012 Elsevier B.V. All rights reserved.

1. Introduction

Many of the materials used in medical technology are polymeric in character with either innate or tailored surface chemistry and morphology which is optimized for specific medical applications [1]. Characterization of the surfaces of such biomaterials and quantitative evaluation of their interaction with relevant proteins, peptides and other biologically active species is an important part of biomaterials optimization. Information from both fundamental and applied studies can aid in determining and understanding the chemical and morphological factors which influence biocompatibility, or lead to adverse interactions, ultimately triggering the foreign body response, thrombus formation *etc.* In general, proteins or peptides are the first species to adsorb to biomaterials and thus much of biomaterials optimization involves controlling protein surface interactions. In this context control may refer to complete prevention or minimization of adsorption (protein resistance, antifouling) or it may refer to the selective promotion of adsorption of one specific protein from the complex mix of species present in the biological tissue or fluid with which the biomaterial is in contact. Maintenance of protein bioactivity is also required in the latter case.

Synthetic materials that are implanted in the body become coated immediately with a layer of proteins [1] either from the adjacent tissue or from blood in the surgical field. This protein layer can stimulate the foreign body response (FBR) leading ultimately to "rejection" of the implant by fibrous encapsulation. The type, amount and conformation of the adsorbed proteins, all of which influence cell adhesion, proliferation and differentiation around the implant, play a role in the FBR [2].

Reduction or elimination of protein adsorption is often desirable for medical devices, while controlled protein adsorption may be important for biochemical sensors [3,4] and nanofluidic systems [5]. Reduction of protein adsorption or controlled adsorption of proteins may be possible by exploiting electrostatic interactions. For instance, nanopatterning of carboxyl-terminated self assembled monolayers (SAMs) with lysozyme for biosensor applications gives protein patterns based on the interaction of the positively charged protein with the negatively charged surface [6]. Repulsive electrostatic interactions can reduce protein adsorption [7] but

* Corresponding author. Tel.: +1 905 525 9140x24749; fax: +1 905 521 2773.
E-mail address: aph@mcmaster.ca (A.P. Hitchcock).
[1] Present address: Alberta Environment and Water, Edmonton, Alberta, T5K 2J6, Canada.

0368-2048/$ – see front matter © 2012 Elsevier B.V. All rights reserved.
http://dx.doi.org/10.1016/j.elspec.2012.06.004

cannot prevent it entirely [8]. Other major driving forces for protein adsorption include, hydrogen bonding, van der Waals forces, and hydrophobic interactions [9].

For the past decade we have been systematically exploring the use of synchrotron based X-ray photoemission electron microscopy (X-PEEM) as a tool for studying biomaterial surfaces and their interactions with relevant proteins and peptides. A comprehensive review of this area of research up to 2009 was recently published [10]. The interested reader is referred to that document for a full description of our past work in the context of other approaches to study these types of systems, as well as descriptions of other X-PEEM applications in biomaterials, such as studies of fluorocarbon coatings on stents [11,12] and copper and polypyrrole micro-patterned substrates [13]. Here, we provide a brief summary of the main themes and outcomes of X-PEEM applied to biomaterials. We compare this approach to other spatially resolved, chemically sensitive methods of surface analysis, and also give a brief exposition of the methodology and present performance of X-PEEM applied to this problem. The main content of this paper is a report on new work dealing with optimization of a polymer blend surface with tunable adsorption behavior. Adsorption data for human serum albumin, a key blood protein, and a SUB-6 (RWWKIWVIRWWR-NH_2), a cationic antimicrobial peptide, are reported for each species alone, and for mixtures of the two, adsorbed to the polymer blend surface. We have chosen to report this study in the context of this special issue on applications of PEEM since it exemplifies most of the themes of our approach – substrate characterization prior to adsorption; quantitative investigation of the adsorption of both small peptides and large proteins; modification of adsorption conditions (in this case by manipulating pH) as a means to learn about the factors controlling adsorption behavior. In addition this surface is the first we have studied which can be intentionally modified in order to tailor its surface adsorption properties through control of surface charge (as reported here) or potentially through chemical functionalization of the reactive acrylic acid groups (planned future work).

Previously, studies of protein adsorption to polystyrene–poly(methyl methacrylate) (PS–PMMA) or PS–polylactide (PLA) films using a synchrotron-based soft X-ray X-PEEM revealed hydrophobic interactions as the dominant adsorption mechanism [14–19]. However, most of the surfaces analyzed thus far with X-PEEM have been neutral and hydrophobic. Here we explore protein and peptide adsorption to a surface prepared by blending PS with a block co-polymer of poly(methyl methacrylate) and polyacrylic acid (PMMA-b-PAA) to form a phase segregated patterned surface that is negatively charged at neutral pH. We report on the chemical composition and surface morphology of PS/PMMA-PAA thin films, and use this system to probe electrostatic interactions with a negatively charged protein and a positively charged peptide as a function of pH.

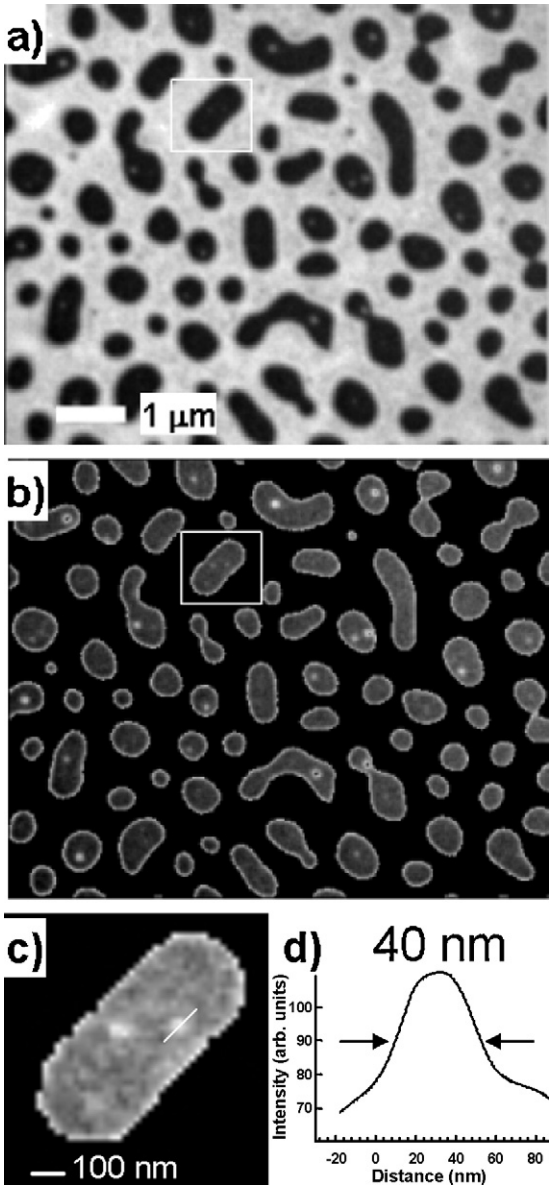

Fig. 1. (a) Image recorded with the ALS PEEM-3 (without the aberration corrector) of a polystyrene–poly(methyl methacrylate) (PS/PMMA) (30/70) blend sample, using a photon energy of 285.15 eV, the C 1s → π* transition of PS. (b) Masked version of (a) to show PS microdomains trapped in the discrete domains of PMMA. (c) Expanded image of the single PMMA domain indicated in (a) and (b). (d) Line profile across the PS microdomain indicating a flat topped character of the 40 nm wide microdomain. The effective spatial resolution is estimated from the edge sharpness to be 30 nm.

2. Overview of X-PEEM applied to protein–polymer interactions

X-PEEM is an ideal tool to map the distribution of protein on polymeric surfaces since this technique combines an optimal near surface sensitivity with a spatial resolution of better than 80 nm. Although techniques such as atomic force microscopy (AFM) [20,21] and transmission electron microscopy (TEM) [22] have better spatial resolution, X-PEEM provides much more detailed chemical information through spatially resolved near-edge X-ray absorption fine structure (NEXAFS) spectroscopy. Scanning transmission X-ray microscopy (STXM) is a comparable technique also capable of using NEXAFS spectroscopy to map biological molecules on surfaces [23,24]. However, STXM operates in transmission mode, which integrates the signal through the entire thickness of the sample, and thus it is much less surface sensitive. For quantitative analyses of surface-adsorbed molecules where the underlying substrate can be mapped simultaneously, X-PEEM is the premier technique. It probes the top 10 nm of the sample, with a sensitivity to adsorbates in the range of 0.1 monolayer or less.

Most of our studies have been performed at the Advanced Light Source (ALS) using the PEEM-2 instrument on beamline 7.3.1. At present the default X-PEEM at the ALS is the PEEM-3 instrument on beamline 11.0.1. Fig. 1a presents an image of a PS/PMMA blend (with molecular weights of 1,000,000 and 300,000 Da respectively) recorded at 285.1 eV with PEEM-3 (operating in PEEM 2.5 mode, without the aberration compensator). Due to improved electron optics the spatial resolution of PEEM-3 is significantly better than that achieved with PEEM-2, as is demonstrated in Fig. 1b–d where

small microdomains of the high molecular weight PS in the lower molecular weight PMMA discrete domains are shown to be imaged with ~30 nm spatial resolution. Since many of the polymers we have studied (especially PMMA and other polymers with ester or acid functional groups) are very radiation sensitive, low flux operation is of greater importance in this research area than spatial resolution. Thus, while the improved spatial resolution of PEEM-3 is very desirable, in our experience it is easier to work at very low flux levels in the PEEM-2 instrument than in the PEEM-3 system.

Fig. 2a presents results from an experimental study of the sampling depth of X-PEEM using NEXAFS spectra of homogeneous thin films of PS with different thicknesses [25]. The increase in the signal from the PS thin film and the decrease of the signal from the Si substrate both saturate at ~10 nm film thickness, which we have thus taken to be the integrated sampling depth. Due to the high extraction field at the sample (>10 kV/mm) and the strong bias for passage of low energy electrons through the PEEM column, the sampling depth is considerably larger than the inelastic mean free path for the primary photoelectron, which is less than 1 nm; rather, the measured 1/*e* fall-off of the signal is 4 nm and the integrated sampling depth is 10 nm. This is very advantageous for biomaterials studies as the sub-monolayer levels of protein or peptide adsorbates, which are the relevant level to probe the critical initial stages of the adsorption process, are sufficiently thin (0.5–5 nm) that the underlying polymer biomaterial also contributes significantly to the detected signal. Thus, X-PEEM is an ideal tool as it can simultaneously detect, quantify and map both adsorbate and substrate.

Fig. 2b–g documents a typical outcome of an X-PEEM study, in this case of a PS/PMMA blend exposed for 20 min to an aqueous solution of human serum albumin (HSA) at a very low concentration (0.005 mg/mL) [16]. The X-PEEM measurement consisted of 43 images, each recorded with a 2 s exposure, with photon energies between 281 and 297 eV. The X-ray beam was shuttered in the 2–3 s interval between each image acquisition in order to reduce radiation damage. After energy calibration, and ratio-ing to the incident photon flux spectrum (determined from a similar image sequence recorded from a clean Si wafer, with correction for the Si X-ray adsorption and a bolometric term relating to the photon energy dependence of the detector), this C 1s image sequence was fit to quantitative C 1s reference spectra of PS, PMMA and HSA (see Fig. 1 of Ref. [19]), which results in maps (Fig. 2b–d) of the spatial distribution of the 3 components within the 10 nm total sampling depth. Fig. 2e is a color coded composite of the 3 component maps which clearly shows that the preferred adsorption sites of the HSA are the interphase region (the ~100–300 nm band between the PS and PMMA domains), followed by PS, with relatively little protein adsorbed on the PMMA domains, as visualized by a relatively pure green color in those areas. In addition to lateral spatial distributions, quantitative amounts (expressed as a thickness in nm) are provided by the data processing. This is accomplished by (i) assuming the total electron yield from the three components is similar (which is plausible given that all components are insulating organic polymers), (ii) establishing a scale factor such that the average of the sum of the component map signals (which are on a quantitative intensity scale relative to each other since the reference spectra are quantitative) is set to 10 nm, and (iii) applying the scale factor to the individual component maps. Fig. 2f displays the map of the sum of the quantitative components. This has much lower contrast variation than the individual component maps, consistent with our assumption that the electron yield and sampling depth are similar across the surface. Fig. 2g displays histograms of the quantitative component maps and the sum, further verifying the reasonableness of our data analysis approach. Further details on sample preparation, measurement protocol and data analysis are provided in Section 3 which describes specific aspects relevant to the main subject of this work.

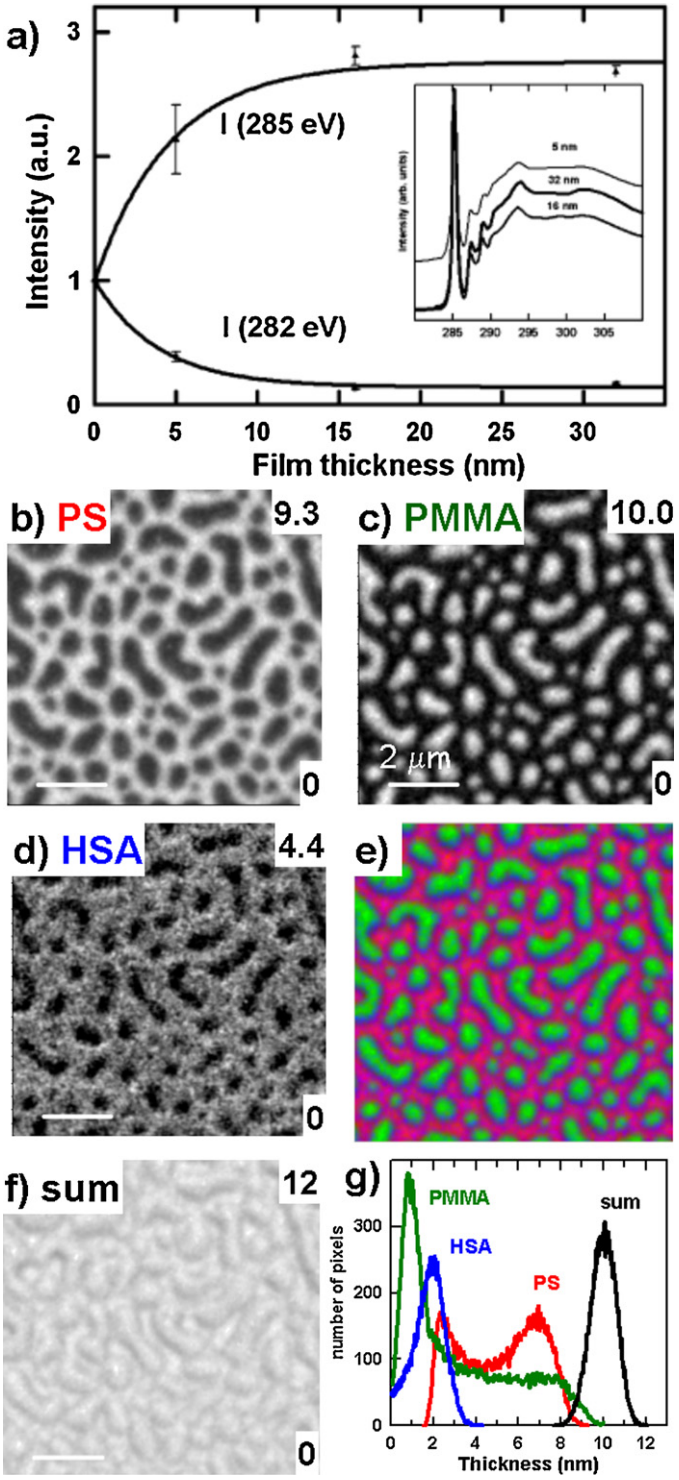

Fig. 2. (a) Plot of intensity at 282 eV (pre-C 1s, sensitive to the Si substrate) and 285 eV (PS peak) as a function of the thickness of spun-coat films of PS [25]. The film thicknesses were measured by atomic force microscopy (AFM) from the profile across a scratch. (b–d) Components maps of a fit of the spectra of PS, PMMA and human serum albumin (HSA) to a C 1s image sequence of a PS/PMMA blend exposed for 20 min to a 0.005 mg/ml aqueous solution of HSA. The number at the top right of each map is the maximum of the gray scale for each component map (in each case the minimum is 0). (e) Rescaled, color coded composite of the PS (red), PMMA (green) and HSA (blue) maps. (f) Sum and (g) histograms of the quantitative component maps. The quantitative thickness scales are established by setting the mean of the sum signal to 10 nm. (For interpretation of the references to color in this figure legend, the reader is referred to the web version of the article.)

The advantages of X-PEEM for biomaterials optimization were outlined above. However, it is also important to discuss its limitations. *In situ* biological experiments using X-PEEM are not possible since relevant biological interactions must be established in an aqueous environment, which is incompatible with the ultra-high vacuum requirement of X-PEEM. One could imagine having an exposure station into which a PEEM sample could be transferred for fluid exposure. However given the need to pump away the fluid prior to returning the sample to the X-PEEM, and other complications, this would not have any particular advantage over the current approach of *ex situ* exposure followed by rinsing, and removal of the final amounts of the water film during the load lock pump down. To avoid charging artifacts, X-PEEM requires ultra-thin samples of the biomaterial. These are not always easy or even possible to prepare. For example polyurethanes are commonly used as medical biomaterials [26] but they, along with other cross-linked polymers, are difficult or impossible to spin coat, which is the preferred technique to prepare polymer films sufficiently thin (<50 nm) to avoid charging in PEEM. Other approaches such as microtoming could be adapted to solve this problem, although PEEM does require very flat surfaces for optimal imaging. It may also be possible to prepare a relevant protein exposed biomaterial on a thick substrate, and then sputter-coat that surface with a layer of metal (Pd, or Pt) that is sufficiently thin to allow electron escape but which is also thick enough to be nearly continuous and sufficiently conducting so as to avoid charging. Gilbert et al. [27,28] have perfected this approach and applied it to many insulating materials, so as to allow studies of thick sections or bulk samples, including many studies of $CaCO_3$ based biominerals (see elsewhere in this special issue). However it is not clear how well adsorbed proteins and delicate organic substrates would survive the energetic sputter coating process.

Currently, it is difficult to use NEXAFS spectroscopy to identify different proteins due to averaging over relatively similar distributions of amino acid residues [29]. Even so, we have successfully studied competitive protein–peptide adsorption in cases where the peptide contains a special spectral signature arising from an abundance of a specific amino acid, in this case, arginine [19]. It may be possible using metal- or quantum-dot-labeled proteins to achieve differentiation of specific components in a mixture of biological adsorbates, although one is always concerned that the label may alter adsorption behavior.

Radiation damage is of considerable concern in these experiments due to the high flux of X-rays, combined with the sensitivity of the organic polymers, proteins and peptides to ionizing radiation. Direct comparison of doses in X-PEEM and STXM [25] have shown that the dose per spectrum is much larger in X-PEEM than in STXM despite the much more concentrated beam in a STXM (typically a spot size of 30 nm diameter with $\sim 10^7$ X-ray/s) than in X-PEEM (typically a spot size of 30 μm diameter with $\sim 10^9$ X-ray/s) because the exposure times in STXM (50–100 ms total per spectrum) are much shorter than in X-PEEM (50–500 s per spectrum). In both types of X-ray microscopes it is now routine to shutter the photon beam except during the actual acquisition step. For X-PEEM the shutter is closed between successive images, while the image is being transferred from the camera to the acquisition computer and the photon energy is being changed. There are clearly improvements that can be made, such as more efficient electron imaging columns, more sensitive cameras, faster data transfer, and more rapid photon shutters. In our present measurement protocol we minimize the exposure by preferentially using the 2-bunch mode which has 1/15th the flux of the normal multi-bunch mode operation. We also mask the incident beam to reduce the flux, and keep the dwell times and number of images measured as low as possible, consistent with spectroscopic differentiation. With the undulator based PEEM-3 at the ALS we have had to extensively detune the EPU to keep the incident flux within the levels that the sensitive PMMA and protein materials can tolerate (see Fig. 1). Sample preparation must also be performed carefully to avoid sharp particulates such as silicon dust from cutting the Si substrate, since they can cause charging and field emission. Finally, despite the zero cost for peer-reviewed access, synchrotron-based techniques are not readily available for many academic or industrial laboratories, due to the limited number of synchrotron facilities and X-PEEM beamlines.

Despite the aforementioned challenges, X-PEEM spectromicroscopy is providing useful information in the biomaterials area. New developments such as aberration correction [30–32] are expected to improve the spatial resolution to ~10 nm in the near future. With 10 nm spatial resolution, imaging individual proteins will become possible. Perhaps more beneficial for this research area, correction of spherical aberration is predicted to increase the transmission of the electron imaging column up to 100-fold which would allow use of smaller apertures in the PEEM column to improve spatial resolution, or enable lower incident fluxes to be used for the same spatial resolution.

3. Materials and methods

3.1. Materials

Polystyrene (MW = 104K, δ 1.05) and poly(methyl methacrylate)-b-polyacrylic acid (MW = 41K–b–10K, δ 1.2) were obtained from Polymer Source Inc. and used as received. Silicon (1 1 1) obtained from Wafer World Inc. was degreased with trichloroethylene, acetone and methanol, followed by rinsing with doubly deionized water (DDI).

Human serum albumin (HSA) was purchased from Behringwerke AG, Marburg, Germany, and found to be homogeneous as judged by sodium dodecyl sulphate polyacrylamide gel electrophoresis (SDS-PAGE). Protein solutions were prepared in DDI water (0.05 mg/mL or 0.005 mg/mL), and the pH was adjusted with HCl or NaOH to 2.0, 4.0 and 8.6. The SUB-6 peptide (RWWKIWVIRWWR-NH_2), a gift from Prof R.E.W. Hancock (University of British Columbia) was prepared using 9-fluorenylmethyl carbamate solid-phase synthesis and purified by high-performance liquid chromatography and mass spectrometry [33].

3.2. Substrates and protein exposure

PS and PMMA-b-PAA were dissolved in dichloromethane in various weight ratios (1 wt%) and films (of varying ratio) were spun cast (4000 rpm, 4 s) onto clean 0.8 cm × 0.8 cm native oxide silicon wafer. The morphology of these substrates was characterized by atomic force microscopy (AFM) and X-ray spectromicroscopy.

The substrates were placed in 50 mL beakers and covered with 5 mL of protein solution. After 20 min, the solutions were diluted with at least 50 mL of DDI water, vigorously rinsed and the remaining water was removed by touching the edge of the Si wafer with lens paper. Since the samples are examined in a ultrahigh vacuum surface analysis system, all of the water is ultimately removed and the samples are examined in a dry state.

3.3. Atomic force microscopy (AFM)

All AFM images were collected with a Quesant Q-scope 250 (Quesant Instruments, Ambios Technology, Santa Cruz, CA), operated in non-contact mode. Standard non-contact silicon cantilevers from Quesant were used. Phase and height mode images (10 μm × 10 μm) were collected simultaneously at a scan rate of 1.8–2.0 Hz under ambient conditions.

3.4. Fluorescence imaging

The spun-cast thin polymer films were treated with a dilute solution of polylysine-fluorescein (40–60K) 1% label in 35 mM HEPES buffer (pH 7.8) which is a treatment that binds specifically to areas of negative charge. The treated samples were examined by optical and fluorescence microscopy using an Olympus BX51 optical microscope fitted with a Q-Imaging Retiga EXi digital camera and ImagePro software. The exposure time was 999 ms.

3.5. STXM

The NEXAFS reference spectra of PS, PMMA, HSA and SUB-6 were collected using a scanning transmission X-ray microscope (STXM) [34,35] at ALS beamline 5.3.2.2 (Berkeley, CA). The PMMA NEXAFS reference spectrum is used in place of PMMA-b-PAA since both PMMA and PAA have intense C 1s → $\pi^*_{C=O}$ transitions at the same position and all other aspects of the NEXAFS spectra of PMMA and PAA are very similar. STXM was used to obtain the reference spectra since STXM has slightly better energy resolution (0.1–0.2 eV) compared to X-PEEM (0.4–0.5 eV); nonetheless, the spectral line shapes from both methods are similar. To minimize radiation damage, the spectra were measured using image sequences [36] and a defocused spot. The intensity scale of each reference spectrum is normalized to the expected theoretical signal of 1 nm of polymer, protein or peptide at its bulk density.

3.6. X-PEEM

The X-PEEM data were collected at the bend magnet beamline 7.3.1 at the ALS using the PEEM-2 microscope. The experimental apparatus, beamline setup and instrument optics are described elsewhere [37]. Briefly, photoelectrons and secondary electrons generated by absorption of circularly polarized monochromatic X-rays are accelerated into an electrostatic imaging column. The spatial distribution of the electrons is magnified and projected on to a phosphor screen which is then imaged by a charged coupled device (CCD) camera. X-PEEM is a partial electron yield technique with high sensitivity for low kinetic energy secondary electrons and an integrated sampling depth for polymers of 10 nm [25].

A 100 nm thick titanium filter was used to eliminate second-order light. To reduce radiation damage, a shutter with a 0.1 s response time was used to block the X-ray beam during each photon energy step as well as the period of transfer of images from the CCD camera to the acquisition computer. The monochromator was masked upstream to reduce the incident flux by 10% and only a limited number of energies (23 at the C 1s edge and very short exposure times (1–5 s) were used to further minimize radiation damage.

4. Results and discussion

4.1. Example of X-PEEM data analysis

The C 1s NEXAFS spectra of all species involved in this study have been presented elsewhere (see Fig. 1 of Ref. [19]). They are readily differentiable so C 1s image sequences provide a suitable tool for chemical mapping. The PS spectrum is characterized by an intense transition at 285.15(3) eV corresponding to the C 1s → $\pi^*_{C=C}$ transition, while the spectra of PMMA and PMMA-b-PAA are dominated by an intense transition at 288.45(3) eV corresponding to C 1s → $\pi^*_{C=O}$ transitions. The characteristic NEXAFS peak of HSA is a strong C 1s → $\pi^*_{C=O}$ transition at 288.20(3) eV which is 0.25(5) eV below the strong C 1s → π^* transition of PMMA or PMMA-b-PAA. This shift is due to the lower electronegative environment of the carbonyl carbon of an amide (in the peptide bond of the protein backbone) as compared to that of the carbonyl carbon of an ester or acid. The C 1s spectrum of the SUB-6 peptide also exhibits a strong C 1s → $\pi^*_{C=O}$ transition at 288.20(3) eV. In addition, SUB-6 has a C 1s → $\pi^*_{C=N}$ transition at 289.37(3) eV and significant intensity in the 286–287 eV region from C 1s(C-R) → $\pi^*_{C=C}$ transitions.

All data analyses were performed with the aXis2000 software package [38]. The C 1s stacks were aligned, normalized to the ring current, and divided by the I_0 spectrum. The I_0 spectrum was obtained from a clean, HF-etched Si(1 1 1) chip and corrected for the absorption of the underlying silicon and a linear energy term representing the bolometric response of X-PEEM detection. The C 1s stacks were calibrated by assigning the C 1s → $\pi^*_{C=C}$ transition of PS to 285.15 eV. While the N 1s NEXAFS spectra have been shown previously to be sensitive to HSA adsorption to polymeric surfaces and a very effective complement to C 1s data [18], N 1s data were not recorded systematically in this project, and thus are not reported in this manuscript.

The C 1s spectrum at each pixel in the stack was fit to the reference spectra of PS, PMMA and HSA/SUB-6 *via* singular value decomposition (SVD) which is an optimized method for least squares analysis in highly over-determined data sets [39,40]. The coefficients obtained from the SVD fit at each pixel are assembled into maps displaying the spatial distribution of each component. Skewed illumination was corrected by dividing a heavily smoothed image obtained from the sum of all component maps. The stack was then divided by a scale factor such that the average total thickness (sum of all components) equaled 10 nm, which is the sampling depth of X-PEEM [25]. The PS, PMMA and HSA component maps are then combined into a single color coded composite map (see Fig. 3a).

A threshold mask was applied to each component map to obtain pixels corresponding to PS, PMMA-b-PAA or the interphase (see as an example, Fig. 3b). Pixels above a certain defined value within each component map were averaged together to obtain a NEXAFS spectrum specific to each region. The spectrum was further modified by setting the pre-edge intensity to zero. This experimental spectrum was then fit to the reference spectra of PS, PMMA and HSA/SUB-6 (see Fig. 3c–e). At least five stacks were obtained from different regions of the same sample and the results of independent analyses of each stack were averaged together. The standard deviation from these multiple determinations was used as an estimate of the uncertainties in the quantitative amounts reported in this work.

4.2. Characterization of the PS/PMMA-b-PAA substrate surface

PS/PMMA-PAA films with mass ratios of 40:60 and 60:40 were spun-cast from dichloromethane (1 wt%) and analyzed with AFM. The phase mode images (Fig. 4a and c) clearly reveal phase segregation with domains in the range of 500 nm–1 μm and 2–4 μm, for the 40:60 and 60:40 films, respectively. The height mode images show the domain heights to be ∼15(5) and ∼20(5) nm, respectively (Fig. 4b and d). The identity of each polymer component is difficult to determine without film destruction [41–43]. Prior to X-PEEM confirmation, the yellow-colored component was tentatively assigned as PMMA-PAA while the orange-colored component was assigned as PS, on the basis of the mass ratios used in preparing the films. As the mass ratio changes from 40:60 to 60:40, a phase inversion occurs with the continuous phase of the 40:60 film, which is yellow in the phase image (Fig. 4a), becoming the discrete domains in the 60:40 film.

The X-PEEM color composite maps (with an absolute intensity scaling) for these two surfaces are shown in Fig. 4e and f with PS color coded in red and PMMA-PAA color coded in green. The X-PEEM maps verify the interpretation of the AFM results, showing that for the 40:60 film, green PMMA-PAA is the continuous phase with embedded red PS domains. The X-PEEM maps for the 60:40

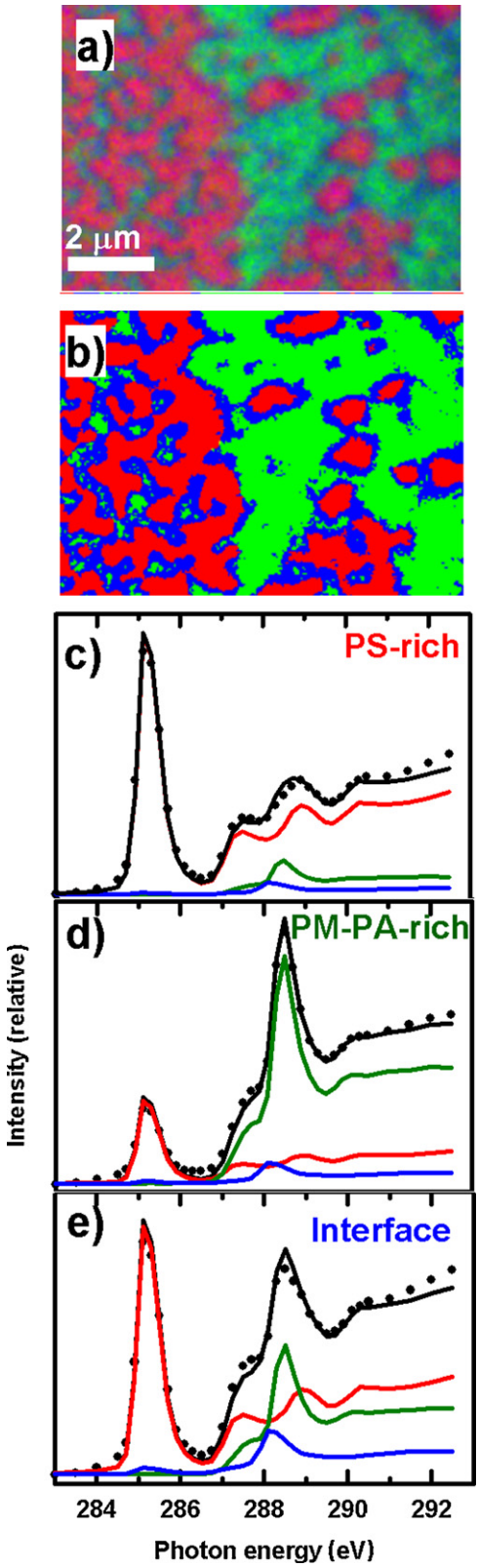

Fig. 3. Example of X-PEEM data and analysis from the PS/PMMA-PAA system. (a) Color coded composite map (non-rescaled) derived from a singular value decomposition (SVD) analysis, using the PS, PMMA and HSA reference spectra (see Fig. 1 of Ref. [19]), of a C 1s image sequence (23 energies) recorded from a PS/PMMA-PAA 60:40 blend thin film spun-cast from a dichloromethane solution with a total loading of 1 wt% polymer with 0.005 mg/mL adsorbed HSA. (b) Mask used to extract spectra of specific regions. Red denotes PS-rich regions, green denotes PMMA-PAA-rich regions, defined by threshold masking the PS and PMMA component maps. The remaining blue pixels define areas at the interphase between the PS-rich and PMMA-rich domains. (c) Curve fit of the average C 1s spectra of the PS-rich region (data, dots; fit, black line; components, colored lines). (d) Curve fit of the average C 1s spectra of the PMMA-PAA-rich region (same symbol and color coding). (e) Curve fit of the average C 1s spectra of the interphase region (same symbol and color coding). (For interpretation of the references to color in this figure legend, the reader is referred to the web version of the article.)

Table 1
Composition of PS and PM–PA (%/pixel) in the PS-rich and PMMA-PAA-rich regions of PS/PMMA-PAA blends with respect to polymer ratio. Uncertainty: ±0.5 nm.

Region	Component	Polymer ratio PS/PMMA-PAA	
		40:60	60:40
PS	PS	8.2	8.3
	PMMA-PAA	1.8	1.7
PMMA-PAA	PS	2.9	1.6
	PMMA-PAA	7.1	8.4

films reveal very small domain sizes with ~100 nm wide PMMA-PAA domains (green) embedded within a continuous phase of PS (red). In addition, these small domains were inter-dispersed with larger PMMA-PAA domains of up to 5 μm in diameter which were apparently pure, as judged by the vivid green color. Thus, it appears that the 10 μm × 10 μm AFM image of the 60:40 film captured only a portion of the PS-rich area.

Quantitative analysis of the X-PEEM results showed the two PS/PMMA-PAA films (40:60 and 60:40) to be reasonable well phase separated (Table 1). For the 40:60 film, the top 10 nm of PS-rich area reveals 8.2(5) nm of PS, while the PMMA-PAA-rich area shows 7.1(5) nm of PMMA-PAA. The phase segregation improved further for the 60:40 film with 8.3(5) nm of PS in the PS-rich area and 8.4(5) nm of PMMA-PAA in the PMMA-PAA-rich area. The improved domainal purity was likely due to the larger domain sizes of the PS/PMMA-PAA 60:40 film which gives a more accurate result due to a lower X-PEEM halo effect (halo refers to the wings of the response function of the X-PEEM electron optics which cause cross-contamination of spectral signals from adjacent areas). The resulting 1.6–1.7 nm of the opposite polymer component is likely the result of small microdomains (~50 nm) which are below the spatial resolution of the PEEM-2 instrument.

Although both the PS/PMMA-PAA 40:60 and 60:40 films are phase segregated, the 60:40 film presents larger domains, which are preferred for protein adsorption studies. Since PAA is negatively charged in neutral aqueous solution, the PS/PMMA-PAA 60:40 film is useful for studying electrostatic interactions. First, investigations of the adsorption of positively charged peptide or negatively charged protein to the negatively charged PS/PMMA-PAA substrate are described. Second, the results of experiments on the effect of changing pH on the protein and peptide adsorption are presented.

The presence of negatively charged PAA at the surface of the film was verified with fluorescence microscopy using polylysine-fluorescein. Reflection and fluorescence images of PS/PMMA-b-PAA 60:40 and pure PMMA as control are presented in Fig. 5. Only surfaces with negative charge are expected to bind the positively charged amino groups of polylysine. The PMMA surface gave no indication of fluorescein binding while the PS/PMMA-b-PAA surface clearly showed fluorescence. The banding patterns reflect deviations from flatness. The phase segregation pattern is seen in the fluorescence image since the PS-rich domains do not bind fluorescein and thus remain black (Fig. 5).

4.3. Protein and peptide electrostatic interactions

At neutral pH, SUB-6 is positively charged (+5) while HSA is negatively charged (−15) [16]. The PS/PMMA-PAA 60:40 substrate was

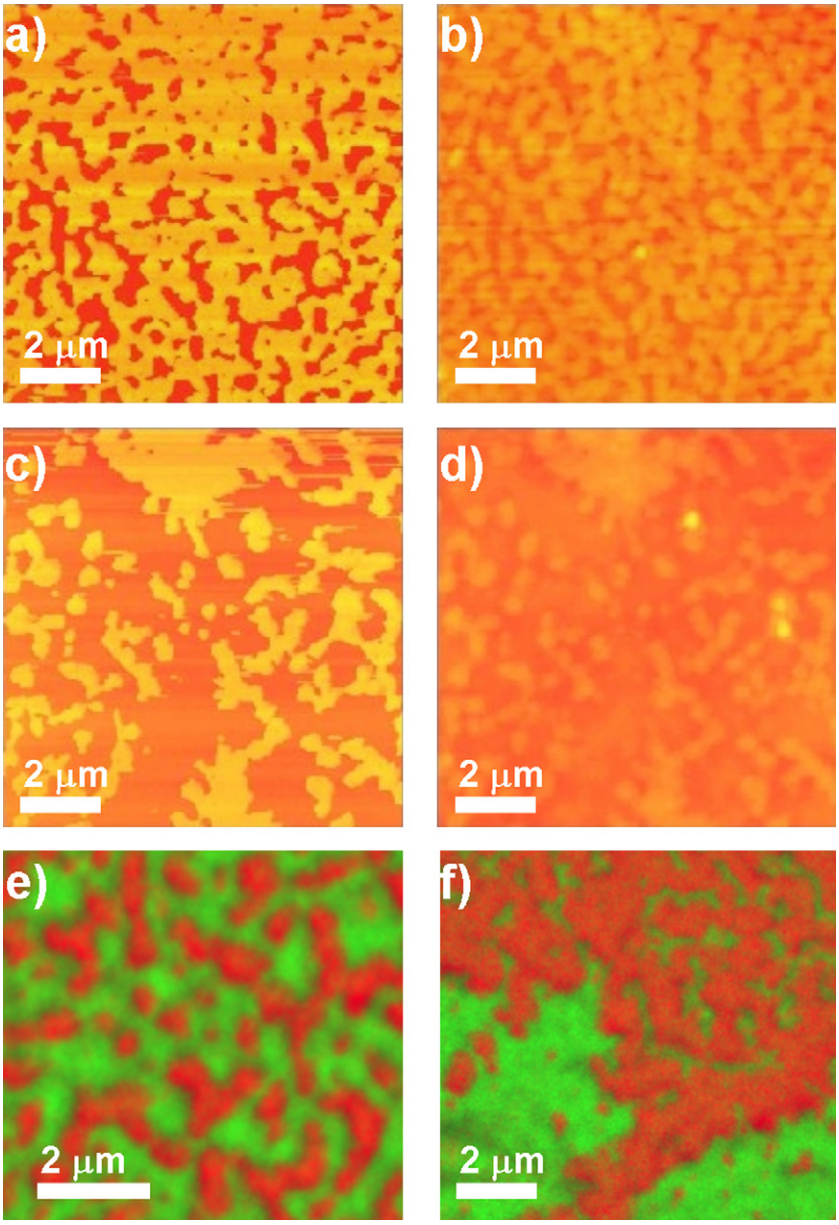

Fig. 4. AFM phase mode images of PS/PMMA-PAA thin film blends spun cast from a 1 wt% dichloromethane solution loaded with (a) 40:60 ratio and (c) 60:40 ratio. AFM height mode images for (b) 40:60 ratio and (d) 60:40 ratio. AFM images are 10 μm × 10 μm. X-PEEM color coded composite maps (rescaled) of PS: PMMA-PAA for (e) 40:60 and (f) 60:40. PS is coded red and PMMA-PAA is coded green. (For interpretation of the references to color in this figure legend, the reader is referred to the web version of the article.)

exposed to either 0.005 mg/mL SUB-6 peptide or 0.005 mg/mLHSA solution for 20 min and then analyzed with X-PEEM. Peptide concentrations of 0.005 mg/mL were used for direct comparison to our previous study of SUB-6 adsorption to PS–PMMA [19].

The color coded composite maps for SUB-6 or HSA adsorption to PS/PMMA-PAA 60:40 are displayed with two presentations (Fig. 6). The maps on the left are rescaled so the intensity of each component (PS, PMMA-PAA and protein/peptide) is mapped to the full 0–255 color range, which is useful for localizing the components. The maps on the right are displayed on an absolute scale (0–10 nm), which preserves the thickness information.

The rescaled color coded image for HSA adsorption to PS/PMMA-PAA is shown in Fig. 6a, with PS, PMMA-PAA and HSA color coded red, green and blue, respectively. HSA adsorption is the strongest on the interdomainal interphase between PS and PMMA-PAA, while the central parts of both the PS and PMMA-PAA domains are relatively pure red and green respectively, indicating very little HSA adsorption. The interdomainal interphase is expected to be region with the highest binding capability due to an amphiphillic character and this would explain these observations if thermodynamics controls the interactions. Alternatively it may be that the interphase is the most "kinetically accessible" at short exposure times, where kinetic factors, such as the rates of transformation of proteins from less favorable to more favorable conformations/orientations for bonding, may play a role [16,17]. The absolute color coded image (Fig. 6b) still shows most protein adsorption at the interphase. The PS and PMMA-PAA regions are even more clearly red and green, respectively, which indicates the overall level of protein adsorption is very low. In contrast, the rescaled image for SUB-6 adsorption to the PS/PMMA-PAA surface also shows the most peptide adsorbed to the interphase (strongest blue color) (Fig. 6c). Both the PS and PMMA-PAA domains show peptide adsorption (pink and teal colors). The absolute image of adsorbed SUB-6 is strongly blue with the highest intensity at the interphase between PS and PMMA-PAA

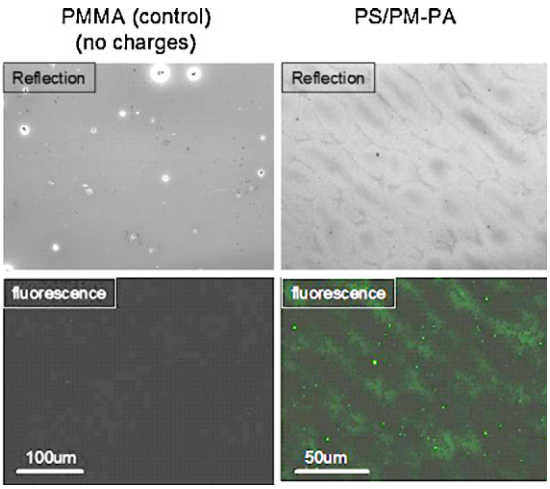

Fig. 5. Optical images of a PMMA control surface (left) and a PS/PMMA-b-PAA 60:40 surface (right), both exposed to polylysine-fluorescence. (Top) Reflection images and (bottom) fluorescence images. Images integrated for 999 ms, gain 5.

(Fig. 6d). Significant adsorption of peptide is evident also on the PS and PMMA-PAA domains. Comparison of the two absolute images (Fig. 6b and d), shows that the adsorption of peptide is significantly greater than that of protein.

The quantitative X-PEEM results are in agreement with the above qualitative analysis, *i.e.* HSA is adsorbed mainly to the interphase (1.6(5) nm) with smaller, approximately equal amounts on the PS and PMMA-PAA (0.7–0.8(5) nm) regions (Table 2). Since both HSA and the surface are net negatively charged, repulsive interactions are expected, and in fact adsorption of HSA to the negatively charged PS/PMMA-PAA surface was more than 50% less than to a PS–PMMA surface (uncharged) at the same concentration [16].

The positively charged SUB-6 peptide shows the opposite adsorption behavior with a large peptide thickness of 4.1–4.2(5) nm

Table 2
Thickness (nm) of PS, PMMA-PAA, and HSA/SUB-6 in the PS, PMMA-PAA and interphase regions for PS/PMMA-PAA 60:40 films exposed to 0.005 mg/mL HSA or SUB-6 in DDI water. Uncertainty: ±0.5 nm.

Region	Composite thickness (nm)	HSA	SUB-6
PS	PS	7.8	6.2
	PMMA-PAA	1.5	0.9
	HSA/SUB-6	0.7	2.9
PMMA-PAA	PS	2.1	1.5
	PMMA-PAA	7.1	4.4
	HSA/SUB-6	0.8	4.1
Interphase	PS	4.9	3.5
	PMMA-PAA	3.5	2.2
	HSA/SUB-6	1.6	4.2

of SUB-6 at the interphase and negatively charged PMMA-PAA domains (Table 2). A peptide thickness of only 2.9(5) nm was observed on the PS-rich areas. Nonetheless, peptide adsorption to the PS/PMMA-PAA surface was much higher than to an uncharged PS–PMMA surface [19]. Indeed the thickness of SUB-6 on the charged surface was greater than on PS/PMMA from a more concentrated solution (0.01 mg/mL): 1.1(5) nm on PS, 3.0(5) nm on PMMA and 4.2(5) nm at the interphase [19]. The increased adsorption of SUB-6 on the PS domains of the charged surface compared to neutral surface is most likely due to adsorption to microdomains of PMMA-PAA embedded within the PS domains.

It seems likely that electrostatic interactions are the driving force for decreased adsorption of HSA and increased adsorption of SUB-6 to the negatively charged surface. A UV–vis spectroscopic study of bovine serum albumin (BSA) and lysozyme adsorption to negatively charged silica particles or positively charged AlOOH-coated silica particles found similar results, with 90–100% of the protein adsorbed to the positively charged surface and almost none (0–10%) to the negative surface [7]. However, both

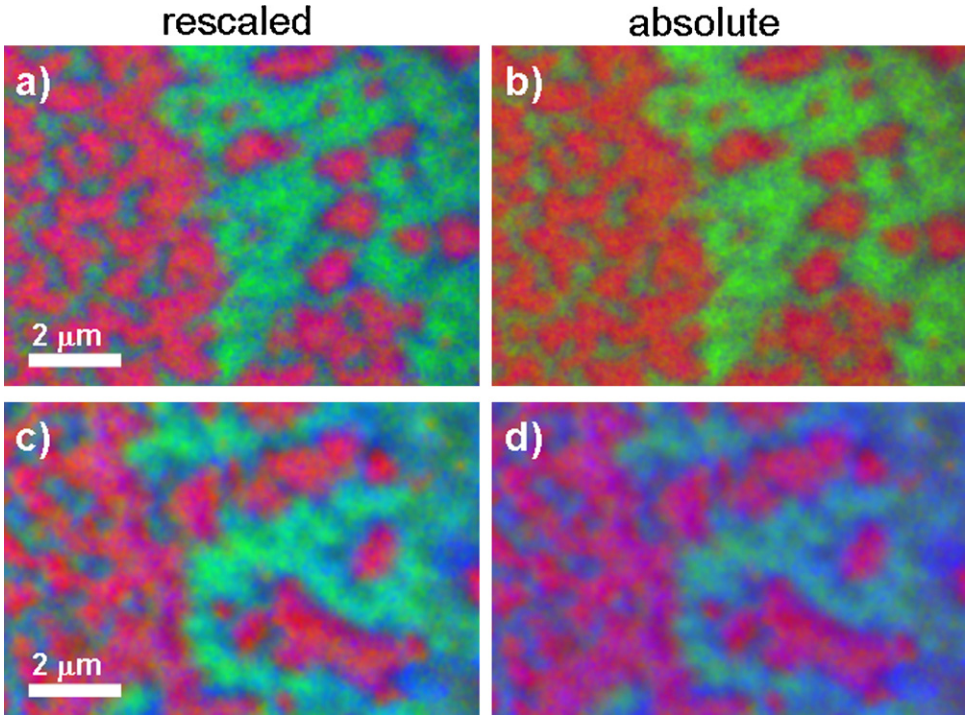

Fig. 6. X-PEEM color coded composite maps of PS/PMMA-PAA 60:40 exposed to 0.005 mg/mL HSA (a) rescaled, (b) absolute, and exposed to 0.005 mg/mL SUB-6 (c) rescaled, (d) absolute. PS is coded red, PMMA-PAA is coded green and HSA/SUB-6 is coded blue. (For interpretation of the references to color in this figure legend, the reader is referred to the web version of the article.)

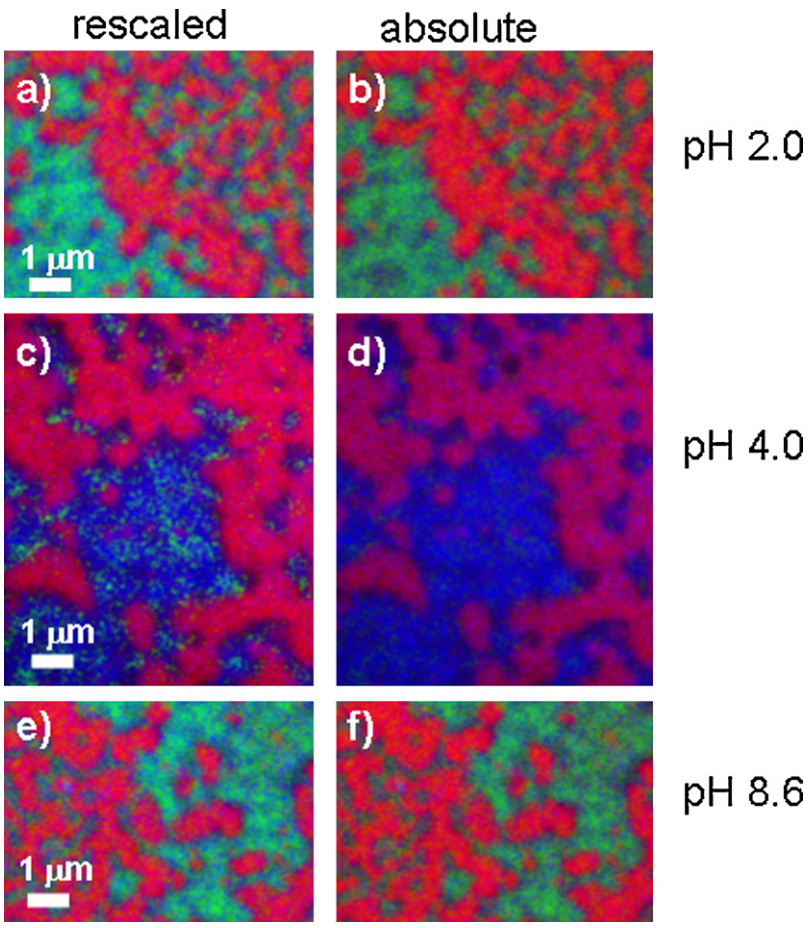

Fig. 7. X-PEEM color coded composite maps of PS/PMMA-PAA 60:40 exposed to 0.05 mg/mL HSA at three different pH values. pH 2.0 (a) rescaled, (b) absolute; pH 4.0 (c) rescaled, (d) absolute; and pH 8.6 (e) rescaled, (f) absolute. PS is coded red, PS-PM is coded green and HSA is coded blue. (For interpretation of the references to color in this figure legend, the reader is referred to the web version of the article.)

AlOOH-coated silica and silica are hydrophilic and thus are not subject to hydrophobic interactions.

In a recent investigation using optical waveguide lightmode spectroscopy (OWLS), α-lactalbumin was found to adsorb to both a negatively charged Nb_2O_5 [44] and a positively charged polylysine surface, even though α-lactalbumin is overall negatively charged at the pH of the experiments [45]. This adsorption was attributed to absorption *via* positive patches on specific parts of the surface of α-lactalbumin despite an overall net negative charge. Hydrophobic or entropic factors were also considered as possible explanations [46]. Similar factors are presumably in play also in the HSA–PS/PMMA-PAA system since HSA adsorption to the negatively charged PS/PMMA-PAA surface was reduced but not eliminated.

4.4. Effect of pH

HSA (0.05 mg/mL) was adsorbed at pH 2.0, 4.0 and 8.6 to PS/PMMA-PAA 60:40 for 20 min. At pH 2, HSA is positively charged while the surface is close to neutral. At pH 4.0, close to the isoelectric point (IP = 4.7–5.3) [47], HSA is slightly positive while the surface is negatively charged. At pH 8.6, both protein and surface are negatively charged. Due to intramolecular charge interactions HSA exists in five different conformations depending on the pH. These are designated E, F, N, B, and A [47]. At lower pH, HSA exists in an unfolded and expanded conformation, while at higher pH it is more compact.

The color composite maps for HSA adsorbed to PS/PMMA-PAA at pH 2.0, 4.0, and 8.6 are presented in Fig. 7. The maps at pH 2.0 (Fig. 7a and b) and 8.6 (Fig. 7e and f) show a strongly blue interphase region, indicating the highest protein adsorption. Similar amounts were adsorbed at pH 2.0 and 8.6 as shown by similar shades of pink PS and teal PMMA-PAA in both maps. Close to the isoelectric point, at pH 4.0, adsorption to the PMMA-PAA region was so high that almost no green PMMA-PA color was visible (Fig. 7b and c). The PS region was also strongly pink showing that adsorption was maximum at pH 4.0.

The estimate of the mean thickness of adsorbed HSA at pH 4.0 on the PS/PMMA-PAA surface was in excess of 4.4(5) nm, with 7.3(5) nm on the PMMA-PAA domains (Table 3). Previous studies have shown that maximum levels of protein adsorption tend to

Table 3
Thickness (nm) of PS, PMMA-PAA, and HSA in the PS, PMMA-PAA and interphase regions for PS/PMMA-PAA 60:40 films exposed to 0.05 mg/mL HSA at pH 2.0, 4.0 and 6.0. Uncertainty: ±0.5 nm.

Region	Component	Composite thickness (nm)		
		pH 2.0	pH 4.0	pH 8.6
PS	PS	7.4	4.8	7.6
	PMMA-PAA	1.1	0.8	0.8
	HSA	1.5	4.4	1.6
PMMA-PAA	PS	2.0	1.4	1.4
	PMMA-PAA	5.4	1.3	1.8
	HSA	2.6	7.3	3.1
Interphase	PS	4.7	4.7	5.2
	PMMA-PAA	2.4	2.8	2.1
	HSA	2.9	5.6	2.7

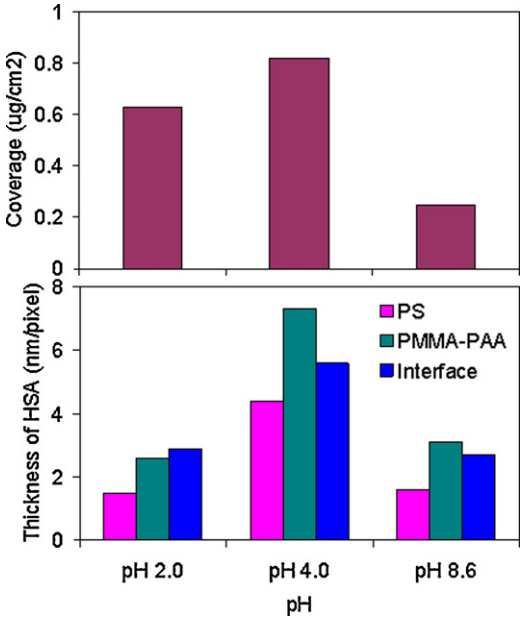

Fig. 8. (Top) ^{125}I radiolabeling experiments of HSA adsorption to PS/PMMA-PAA 60:40 as a function of pH, compared to (bottom) X-PEEM detected thicknesses. Pink denotes HSA thickness on PS, teal denotes HSA thickness on PMMA-PAA and blue denotes HSA thickness at the interphase. (For interpretation of the references to color in this figure legend, the reader is referred to the web version of the article.)

Table 4
HSA adsorption to PS/PMMA-PAA surface at varying pH (^{125}I radiolabeling).

pH	Adsorption[a]	Std Dev (n = 4)
2	0.628	0.076
4	0.819	0.022
8.6	0.245	0.092

[a] μg/cm^2 from DDI water.

occur at the isoelectric point where the protein carries no charge and thus exhibits least electrostatic repulsion [1–4]. Since HSA has dimensions of 8 nm × 8 nm × 3 nm [48] it appears either to be adsorbing predominantly end-on or to be forming partial bilayers. Measurement of adsorption to PMMA-PAA using radiolabeling gave a value of 0.701 μg/cm^2. For end on adsorption (8 nm × 3 nm footprint) approximately 0.46 μg/cm^2 is equivalent to a close packed monolayer. However at pH 4.0 it is known that HSA exists in an expanded conformation, so that a monolayer should contain less than 0.46 μg/cm^2. The data in Table 3 thus suggest that the layer of HSA on the PMMA-PAA region at pH 4.0 is partly monolayer and partly bilayer.

HSA adsorption at pH 2.0 and 8.6 was significantly less than at pH 4.0 with thickness estimates at pH 2.0 and 8.6 in the range of 1.5–3.1(5) nm. At pH 4.0, adsorption on PS/PMMA-PAA was significantly higher presumably due to attractive electrostatic interactions. Compared to the (uncharged) PS/PMMA surface, adsorption on PS/PMMA-PAA was two- to three-fold greater [17]. At pH 8.6, where HSA is negative, adsorption to the negative PS/PMMA-PAA surface was much greater than to the uncharged PS/PMMA surface. However the thickness value obtained for the uncharged surface (∼1 nm) was low, especially when compared to the radiolabeling results [17].

As seen in Table 3, the adsorbed HSA thicknesses at pH 8.6 and 2.0 were similar. The same trend was seen in radiolabeling experiments reported earlier for HSA adsorption to PS/PMMA. Adsorption of 0.117, 0.223, and 0.130 μg/cm^2 at pH 2.0, 4.0 and 8.6, respectively was observed [14]. Results of radiolabeling experiments at varying pH are presented in Fig. 8 and Table 4. From the Mann–Whitney U rank sum test, we found a statistically significant difference between the results for adsorption at pH 2 compared to those at pH 4 (p = 0.02). Furthermore, there is also a statistically significant difference between the absorption at pH 4 compared to pH 8 (p = 0.02). The overall trend was similar to that seen in the X-PEEM data, with maximum adsorption near the isoelectric point. The adsorbed quantities on negative PS/PMMA-PAA were significantly higher than on neutral PS/PMMA at all three pH values [17].

Interestingly, the X-PEEM-determined thicknesses at pH 2.0 and 8.6 were similar, while the adsorbed amount at pH 2 measured by radiolabeling was greater by a factor of ∼3. At pH 2.0 HSA is in an extended conformation while at pH 8.6 the conformation is compact. It seems possible that the different conformations may result in layers of similar thickness but different adsorbed quantity.

5. Conclusions

X-PEEM and AFM were used to investigate the surface morphology of PS/PMMA-PAA spun cast thin films. It was found that the top 10 nm of the film surface was phase segregated. The adsorption to these films of HSA and SUB-6 peptide, negatively and positively charged, respectively, at neutral pH, appeared to be driven at least in part, by electrostatic interactions as indicated by experiments at varying pH. Adsorbed quantities measured by ^{125}I-radiolabeling at varying pH showed similar trends to the X-PEEM data. These results, along with others from more than a decade of research in this area [10], demonstrate the power of X-PEEM applied to fundamental and applied studies of biomaterial surfaces and their interactions with biological molecules.

Acknowledgements

We gratefully thank the Hancock Research Group from UBC for their gift of SUB-6 peptide. We acknowledge fruitful discussion with K. Leung on statistical analyses. This research is supported by the Natural Sciences and Engineering Research Council (NSERC, Canada), AFMNet and the Canada Research Chairs program. X-ray microscopy was carried out using PEEM-2 and STXM5322 at the ALS. The ALS is supported by the US Department of Energy under Contract DE-AC03-76SF00098.

References

[1] D.G. Castner, B.D. Ratner, Surf. Sci. 500 (2002) 28.
[2] J.M. Anderson, A. Rodriguez, D.T. Chang, Semin. Immunol. 20 (2008) 86.
[3] B.L. Frey, C.E. Jordan, S. Komguth, R.M. Com, Anal. Chem. 67 (1995) 4452.
[4] M. Veiseh, M.H. Zareie, M. Zhang, Langmuir 18 (2002) 6671.
[5] L.S. Roach, H. Song, R.F. Ismagilov, Anal. Chem. 77 (2005) 785.
[6] K. Wadu-Mesthrige, S. Xu, N.A. Amro, G.Y. Liu, Langmuir 15 (1999) 8580.
[7] K. Rezwan, L.P. Meier, L.J. Gauckler, Biomaterials 26 (2005) 4351.
[8] W. Norde, J. Lyklema, J. Biomater. Sci. Polym. Ed. 2 (1991) 183.
[9] C.A. Haynes, W. Norde, Colloids Surf. B 2 (1994) 517.
[10] B.O. Leung, J.L. Brash, A.P. Hitchcock, Materials 3 (2010) 3911.
[11] P. Hale, S. Turgeon, P. Horny, F. Lewis, N. Brack, G. Van Riessen, P. Pigram, D. Mantovan, Langmuir 24 (2008) 7897.
[12] P. Chevallier, S. Holvoet, S. Turgeon, P. Horny, J.J. Pireaux, D. Mantovani, J. Appl. Polym. Sci. 118 (2010) 3176.
[13] P. Kappen, P.S. Hale, N. Brack, W. Prissanaroon, P.J. Pigram, Appl. Surf. Sci. 253 (2006) 1473.
[14] B.O. Leung, A.P. Hitchcock, J.L. Brash, A. Scholl, A. Doran, Macromolecules 42 (2009) 1679.
[15] C. Morin, A.P. Hitchcock, R.M. Cornelius, J.L. Brash, a. Scholl, A. Doran, J. Elecctron Spectrosc. 137–140 (2004) 785.
[16] L. Li, A.P. Hitchcock, N. Robar, R. Cornelius, J.L. Brash, A. Scholl, A. Doran, J. Phys. Chem. B 110 (2006) 16763.
[17] L. Li, A.P. Hitchcock, R. Cornelius, J.L. Brash, A. Scholl, A. Doran, J. Phys. Chem. B 112 (2008) 2150.
[18] B.O. Leung, A.P. Hitchcock, R.M. Cornelius, J.L. Brash, A. Scholl, A. Doran, Biomacromolecules 10 (2009) 1838.
[19] B.O. Leung, A.P. Hitchcock, J.L. Brash, A. Scholl, A. Doran, P. Henklein, J. Overhage, K. Hilpert, J.D. Hale, R.E.W. Hancock, Biointerphases 3 (2008) F27.

[20] C.A. Siedlecki, R.E. Marchant, Biomaterials 19 (1998) 441.
[21] T.C. Ta, M.T. McDermott, Anal. Chem. 72 (2000) 2627.
[22] A. Sousa, M. Sengonul, R. Latour, J. Kohn, M. Libera, Langmuir 22 (2006) 6286.
[23] B.O. Leung, J. Wang, J.L. Brash, A.P. Hitchcock, Langmuir 25 (2009) 13332.
[24] A.P. Hitchcock, C. Morin, Y.M. Heng, R.M. Cornelius, J.L. Brash, J. Biomater. Sci. Polym. Ed. 13 (2002) 919.
[25] J. Wang, L. Li, C. Morin, A.P. Hitchcock, A. Doran, A. Scholl, J. Electron Spectrosc. 170 (2009) 25.
[26] L.-C. Xu, J. Runt, C.A. Siedlecki, Acta Biomater. 6 (2010) 1938.
[27] B. Gilbert, G. Margaritondo, S. Douglas, K.H. Nealson, R.F. Edgerton, G. Rempfer, G. De Stasio, J. Electron Spectrosc. Relat. Phenom. 114/116 (2001) 1005.
[28] G. De Stasio, B.H. Frazer, B. Gilbert, K.L. Richter, J.W. Valley, Ultramicroscopy 98 (2003) 57.
[29] J. Stewart-Ornstein, A.P. Hitchcock, Daniel Hernàndez-Cruz, P. Henklein, J. Overhage, K. Hilpert, J. Hale, R.E.W. Hancock, J. Phys. Chem. B 111 (2007) 7691.
[30] R. Wichtendahl, R. Fink, H. Kuhlenbeck, D. Preikszas, H. Rose, R. Spehr, P. Hartel, W. Engel, R. Schlögl, H.-J. Freund, A.M. Bradshaw, G. Lilienkamp, Th. Schmidt, E. Bauer, G. Brenner, E. Umbach, Surf. Rev. Lett. 5 (1998) 1249.
[31] P. Schmid, J. Feng, H.A. Padmore, D. Robin, H. Rose, R. Schlueter, W. Wan, E. Forest, Y. Wu, Rev. Sci. Instrum. 76 (2005) 023302.
[32] A.A. MacDowell, J. Feng, A. DeMello, A. Doran, R. Duarte, E. Forest, N. Kelez, M.A. Marcus, T. Miller, H.A. Padmore, S. Raoux, D. Robin, A. Scholl, R. Schlueter, P. Schmid, J. Stohr, W. Wan, D.H. Wei, Y. Wu, AIP Conf. Proc. (2007) 1341.
[33] D. Romeo, B. Skerlavaj, M. Bolognesi, R. Gennaro, J. Biol. Chem. 263 (1988) 9573.
[34] T. Warwick, H. Ade, A.L.D. Kilcoyne, M. Kritscher, T. Tylisczcak, S. Fakra, A.P. Hitchcock, P. Hitchcock, H.A. Padmore, J. Synch. Rad. 9 (2002) 254.
[35] A.L.D. Kilcoyne, T. Tylisczak, W.F. Steele, S. Fakra, P. Hitchcock, K. Franck, E. Anderson, B. Harteneck, E.G. Rightor, G.E. Mitchell, A.P. Hitchcock, L. Yang, T. Warwick, H. Ade, J. Synch. Rad. 10 (2003) 125.
[36] C.J. Jacobsen, C. Zimba, G. Flynn, S. Wirick, J. Microsc. 19 (2000) 173.
[37] S. Anders, H.A. Padmore, R.M. Duarte, T. Renner, T. Stammler, A. Scholl, M.R. Scheinfein, J. Stohr, L. Seve, B. Sinkovic, Rev. Sci. Instrum. 70 (1999) 3973.
[38] aXis2000 is free for non-commercial use. It is written in Interactive Data Language (IDL) and available from http://unicorn.mcmaster.ca/aXis2000.html.
[39] G. Strang, Linear Algebra and its Applications, Harcourt Bracourt, Jovanovich, San Diego, 1988.
[40] I.N. Koprinarov, A.P. Hitchcock, C.T. McCrory, R.F. Childs, J. Phys. Chem. B 106 (2002) 5358.
[41] P. Wang, J.T. Koberstein, Macromolecules 37 (2004) 5671.
[42] S. Walheim, M. Ramstein, U. Steiner, Langmuir 15 (1999) 4828.
[43] N. Virgilio, B.D. Favis, M.F. Pepin, P. Desjardins, G. L'Esperance, Macromolecules 38 (2005) 2368.
[44] S. Pashe, J. Voros, H.J. Griesser, N.D. Spencer, M. Textor, J. Phys. Chem. B 109 (2005) 17545.
[45] T. Arai, W. Norde, Colloids Surf. 51 (1990) 1.
[46] N. Fogh-Andersen, P.J. Bjerrum, O. Siggaard-Andersen, Clin. Chem. 39 (1993) 38.
[47] J.F. Foster, in: V.M. Rosenoer, M. Oratz, M.A. Rothschild (Eds.), Albumin Structure, Function and Uses, Pergamon, Oxford, 1977, pp. 53–84.
[48] S. Sugio, A. Kashima, S. Mochizuki, M. Noda, K. Kobayashi, Protein Eng. 12 (1999) 439.